Hardness–Tensile Property Relationships for HAZ in 6061-T651 Aluminum

Hardness is a reliable method of characterizing the tensile strength of the HAZ; relationships between hardness and tensile properties were established

P. A. STATHERS, A. K. HELLIER, R. P. HARRISON, M. I. RIPLEY, AND J. NORRISH

ABSTRACT

High-strength aluminum is used extensively in industry, with welding being a widely used fabrication method. This work focuses on welding of 6061-T651 aluminum and establishment of the hardness–tensile properties relationship in the heat-affected zone (HAZ) of a gas metal arc weld using 4043 filler material. Test welds were prepared from 12.7-mm-thick plate with a single-V weld preparation. Base plate temperatures were measured with an array of eight embedded thermocouples during welding, relating temperature to properties at intervals from the weld. Through-thickness slices 1.7 mm thick were removed, by electric discharge machining, from the plate parallel to the weld at 2-mm intervals and extending from the weld centerline to 40 mm into the HAZ and base plate. Tensile samples were prepared from these slices, and tensile properties and hardness values measured to establish a relationship between these two parameters. Both EQUOTIP (portable hardness tester) and Vickers microhardness measurements were conducted and related to tensile properties. Although a significant body of work exists relating tensile properties to hardness, no previous study was found that used this approach. Most work appeared to use cross-weld tensile tests, which only give the point of lowest strength. Sections of base plate material having a different thickness (31.75 mm) from that of the welded samples, and from a different source, were thermally aged to four hardness values and the hardness–tensile relationship was also established for this material. These results were compared with those of the HAZ samples; the results were found to fall within the scatter band of HAZ results.

KEYWORDS

•6061-T651 Aluminum Alloy • 4043 Filler Metal • Gas Metal Arc Welding (GMAW) • Gas Tungsten Arc Welding (GTAW)• Heat-Affected Zone (HAZ) • Weld Metal • Vickers Microhardness Test • EQUOTIP Portable Hardness Tester • Tensile Properties

Introduction

Alloy 6061 belongs to the 6XXX series of wrought heat-treatable aluminum alloys. These are of the (Al-Mg-Si) ternary system, in which magnesium and silicon are the major alloying constituents; they can also be thermodynamically approximated as a pseudo-binary (Al-Mg_2Si) system. Alloy 6061-T651 is solution heat-treated, quenched, stress-relieved by stretching, and then artificially aged to peak hardness. By solution heat-treating and quenching the alloy, it subsequently produces a supersaturated solid solution, a relatively soft structure that exists in a thermodynamically metastable state. If this is followed by an aging heat treatment, it induces precipitation of the excess solute atoms and, ultimately, the dissociation of the supersaturated solid solution into the equilibrium β phase. It is the precipitation of these excess solute atoms that provides the alloy with enhanced strengthening properties, by acting as barriers to dislocation movement. Peak hardness is associated with the combination of the intermediate phases β" and β′. However, alloys aged beyond peak hardness experience a decrease in hardness associated with an increase in the interparticle spacing between precipitates, which makes dislocation bowing much easier. This is commonly referred to as the overaged condition. Porter and Easterling (Ref. 1) have reported that increasing the time and/or temperature used for heat treatment of a system subsequently induces an increase in the driving force for precipitation and precipitate coarsening. Dumolt et al. (Ref. 2) as well as Enjo and Kuroda (Ref. 3) associate the softening of the alloy with the transformation of β″ phase into the β′ phase with increasing aging time and/or temperature. The Ostwald ripening of precipitates increases the interparticle spacing, giving a more coarse dispersion

P. A. STATHERS was materials engineer, R. P. HARRISON is program leader, Structural Integrity, and M. I. RIPLEY is visiting fellow at the Institute of Materials Engineering, Australian Nuclear Science and Technology Organisation, Lucas Heights, NSW, Australia. A. K. HELLIER is visiting fellow, School of Mechanical and Manufacturing Engineering, The University of New South Wales, Sydney, Australia. J. NORRISH is professor, Materials Welding and Joining in the Faculty of Engineering, University of Wollongong, Australia.

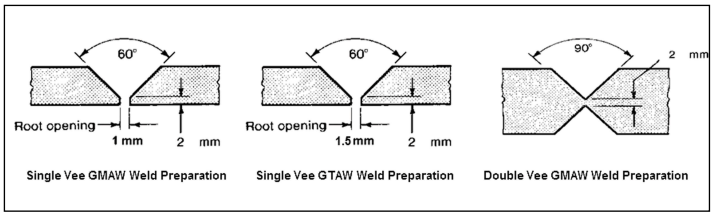

Fig. 1 — Weld preparations for test plates.

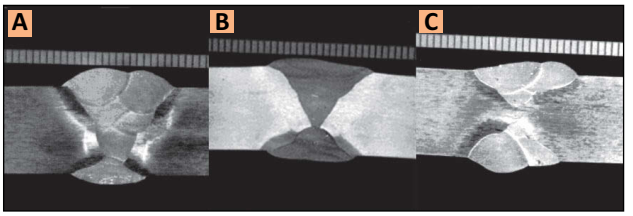

Fig. 2 — Macrographs of welded plates. Scales are in mm. A — Plate 2A (single-V GMA weld); B — Plate 2B (single-V GTA weld); C — Plate 2C (double-V GMA weld).

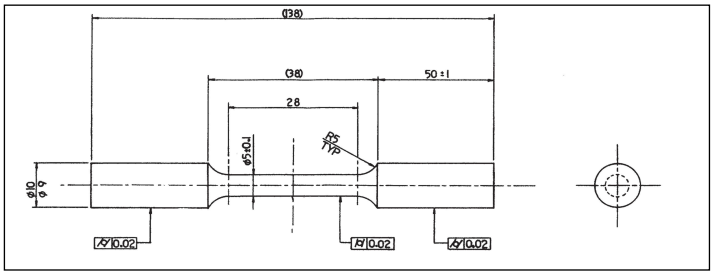

Fig. 3 — Tensile sample design. Overaged base plate (Plate 1). Dimensions are in mm.

as a result of the bigger, more stable precipitates consuming the smaller, less stable precipitates surrounding them.

Welding is a popular method of joining 6061 aluminum (Ref. 4) and it has been demonstrated (Refs. 5-7) that the heat-affected zone (HAZ) and the fusion zone metal have lower strengths (softening) resulting from the welding process, if welded in the T6 condition. This process of overaging occurs because the microstructure has been modified by exposure to a temperature/time regime that produces less than optimal strength. These weld-induced changes in properties influence the design of structures: the designer must take into account the magnitude of the change in properties, and the location and orientation of the weld with respect to the direction of applied stress. Although hardness measurements have long been used to indicate the extent of the HAZ in welds (Ref. 8), no systematic study could be found that attempts to relate hardness to measured properties on a single weld metal and accompanying HAZ. The relationship between hardness and yield stress for all alloy systems in general is well established (Ref. 9), but that between hardness and other tensile properties is less so. The present paper is taken from the experimental work in the dissertation of Ref. 10 and is aimed at providing a model relating tensile properties to hardness in the 6061-T651 base plate–4043 filler metal combination by sectioning thin zones of the weld and HAZ.

Although taking out microtensile specimens at different locations from the welded plate is an original approach, mention should be made of an alternative method using Gleeble machine experiments in which it is possible to reproduce the thermal cycles at any location in the HAZ, thereby producing a tensile specimen with more or less homogeneous material properties. These types of experiments are used to verify numerical models and the results from this activity are extensively published (Refs. 11–22). Such models can be coupled with a finite element code, e.g., WELDSIM™ (Refs. 23, 24), to calculate material properties at any location in the HAZ as a function of welding parameters and geometry of the welded parts. These calculations are more or less standard procedure at Hydro Aluminium Structures, N-2831, Raufoss in Norway, for welded automotive components. However, from a practical standpoint, hardness measurements are quicker and more straightforward than numerical calculations of the HAZ properties.

Previous workers, e.g., Malin (Ref. 25), used cross-weld test samples as the basis for the hardness–tensile relationship, the position of the break on the tensile sample being related to its location with respect to the weld. The present work examines the tensile properties at 2-mm (0.079-in.) intervals from the center of the weld to

Table 1 — Conversions from SI Units to U.S. Customary Units

SI Unit	Conversion Factor	U.S. Customary Unit
1 millimeter (mm)	≈ 0.0393701	inch (in.)
1 meter (m)	≈ 3.28084	foot (ft)
1 milliliter (mL)	≈ 0.0338140	fluid ounce (U.S.)
1 liter (L)	≈ 0.264172	gallon (U.S.)
1 kilogram (kg)	≈ 2.20462	pound (lb)
1 kilonewton (kN)	≈ 0.224809	kilopound-force (kip)
1 megapascal (MPa)	≈ 0.145038	kilopound-force per square inch (ksi)
±1 deg Celsius (°C)	= 9/5	± deg Fahrenheit (°F)

Temperature in deg Fahrenheit (°F) = 9/5 x temperature in degrees Celsius (°C) + 32

Table 2 — Test Plate Material Specification

Plate No.	Alloy	Thickness (mm)	Specification	Lot No.	As-Supplied Hardness EQUOTIP L_D	Vickers HV(20)
1A	6061-T651	31.75	ASM QQA-250/11	Lot 304831	456	112
2	6061-T651 Type 200	12.7	ASM QQA-250/11	#681-417 Alcoa	465	114

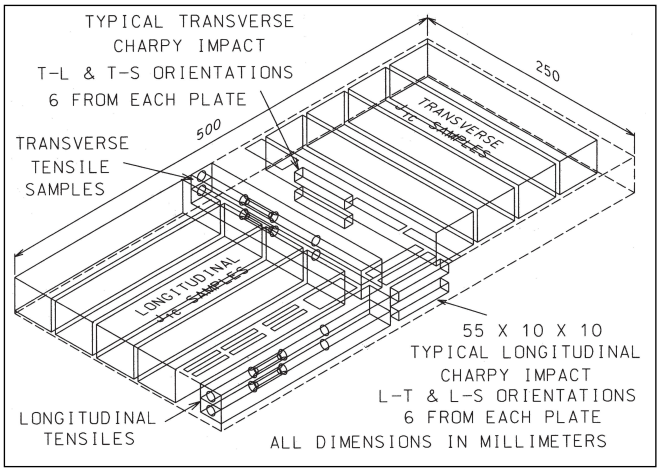

Fig. 4 — Overaged base plate (Plates 1—A1 to A4) sample removal locations. Note that only the tensile samples were used in the present work reported in this paper.

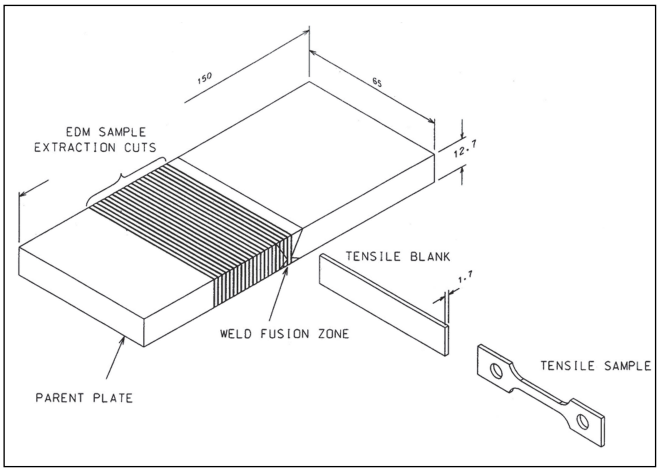

Fig. 5 — Extraction layout for HAZ samples removed from Plate 2A. Dimensions are in mm.

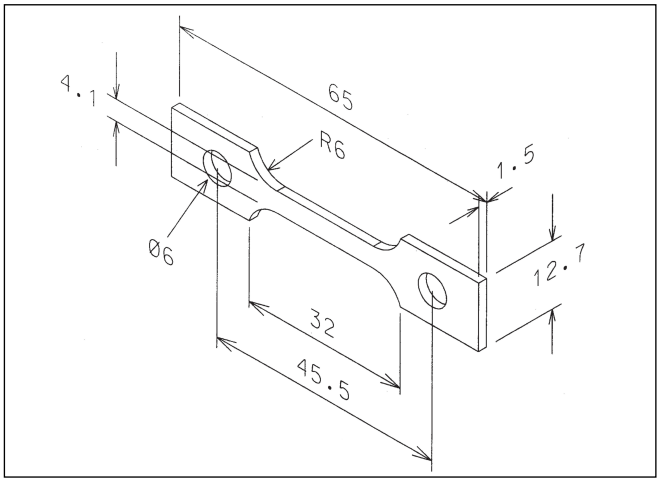

Fig. 6 — HAZ tensile sample design. Dimensions are in mm.

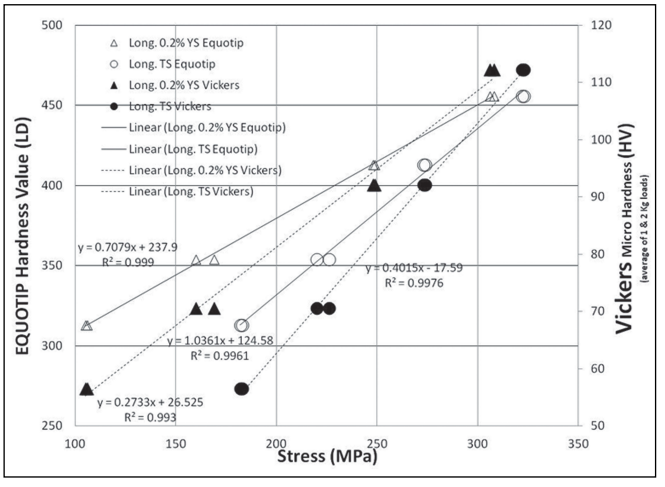

Fig. 7 — Overaged base plate (Plate 1). Longitudinal 0.2% yield stress and tensile strength as a function of EQUOTIP and Vickers hardness.

the unaffected base metal. Table 1 contains all necessary conversions from SI units to U.S. customary units.

Experimental Materials

Specification

Two thicknesses of plate were used: 31.75 mm (1.25 in.) and 12.7 mm (0.5 in.). The 31.75-mm plate is referred to as Plate 1 and the 12.7-mm plate, Plate 2. Both plates were supplied to the same specification (ASM-QQA-250/11) and were provided in the T651 temper. Table 2 gives details of the plate and initial hardness reading from each plate. Table 3 gives the chemical analysis of the two test plates as well as the nominal composition of the alloy for comparison. The Zn content of Plate 1 was found to be out of specification; however, the small deviation is not expected to affect the mechanical properties to any significant extent.

Both plates supplied were factory-marked at regular intervals along their length with alloy, temper, specification, and lot number for secu-

Table 3 — Chemical Analysis of Test Plates (wt-%)

Test Plate	Si	Cu	Fe	Mg	Zn	Cr	Mn	Ti	Ni	Sr	Zr	Al
1	0.67	0.30	0.61	1.05	0.42	0.20	0.10	<0.01	<0.01	<0.001	<0.005	Bal
2	0.6	0.24	0.45	0.95	0.01	0.19	<0.01	0.03	<0.01	<0.001	<0.005	Bal
Nominal Composition	0.4–0.8	0.15–0.40	0.7 max	0.8-1.2	0.25 max	0.04–0.35	0.15 max	0.15 max	Other elements no more than 0.05% each, 0.15% total			Bal

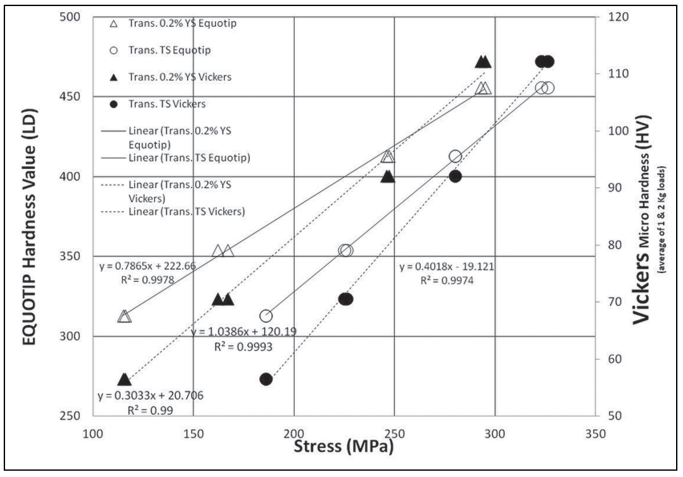

Fig. 8 — Overaged base plate (Plate 1). Transverse 0.2% yield stress and tensile strength as a function of EQUOTIP and Vickers hardness.

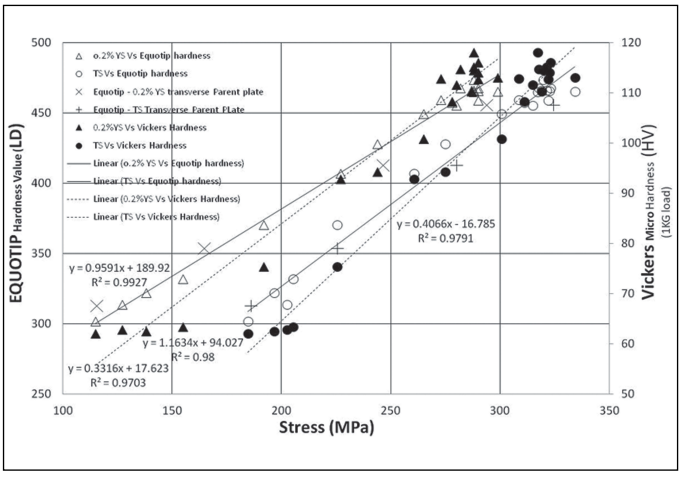

Fig. 9 — HAZ through-thickness tensile sample results vs. EQUOTIP hardness and Vickers microhardness, GMA weld (Plate 2A).

Table 4 — Base Plate Heat Treatments and Hardnesses

Plate Number	Temperature (°C)	Time (h)	EQUOTIP Hardness L_D	Vickers Hardness HV(20)
1–A1	As-received material		456	110
1–A2	247	0.7	413	91
1–A3	260	9.5	354	71
1–A4	260	9.5		
	270	65		
	300	2.5	313	57

Table 5 — Summary of Welded Test Plates

Plate	Thickness (mm)	Weld Preparation (as per Fig. 1)	Welding Method	Weld Procedure Sheet No. (see Appendix 1 in Ref. 10)
2A	12.7	Single Vee	GMAW Pulsed	WP1
2B	12.7	Single Vee	GTAW AC	WP2
2C	12.7	Double Vee	GMAW Pulsed	WP3

rity of identification. Subdivisions of the original 31.75-mm plate were assigned an alphabetical postscript (A and B); further subdivisions were assigned a further numerical subdivision (Plate 1 — A1, A2, A3, A4) and test samples produced from these plates were assigned individual test code numbers (TXXXX).

Filler Metal

A new spool of 4043 filler metal was used to weld the gas metal arc welded (GMAW) test plates. The spool of 1.6-mm wire had been sealed until use. Gas tungsten arc welds (GTAW) were prepared using 2.5-mm-diameter 4043 filler metal.

Experimental Procedure

Overaging of Test Plates

The objective was first to produce four plates with different hardnesses by overaging heat treatments. Hardness vs. tensile properties were then obtained using full-size tensile samples. These results were compared with values obtained from the subsize tensile test pieces extracted from the welded plates, to ensure that there were no sample size effects.

Plate 1A was cut into four pieces, each measuring approximately 500 × 250 mm. Three of these were heat treated to overage the material to various hardnesses. Type K thermocouples were attached to the plates to monitor their surface temperatures during heat treatment. Heating times and temperatures are shown in Table 4 together with the hardnesses measured for each plate.

Preparation of Welded Test Plates

Three welded test plates were prepared in accordance with the recommendations in AS 1664 (Ref. 26); Table 5 summarizes the preparation and welding method used in each case. Details of the weld preparation for both types of test plate (single- and double-V) are shown on the weld procedure sheets for each weld — Fig. 1.

Welding Procedure

Gas metal arc welding was performed using a Synchro-pulse CDT Model No. CP 34 welding unit manufactured by Welding Industries of Australia (WIA). This unit uses a square wave pulsed waveform. A copper backing bar, 100 mm wide by 6 mm thick, was fitted under the single-V weld preparation. The weld preparations and interpass regions were thoroughly cleaned with acetone and stainless steel wire brushing immediately prior to welding. The shielding gas was welding grade argon at a flow rate of 26 L/min. The single-pass GMA weld was mechanically back-machined to a depth of 4 mm to remove any defects in the root run; this groove was then filled with a single weld pass.

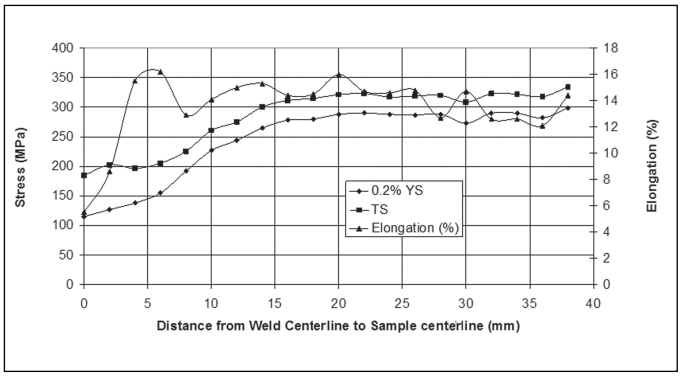

Fig. 10 — HAZ through-thickness tensile sample results vs. distance from weld centerline, GMA weld (Plate 2A).

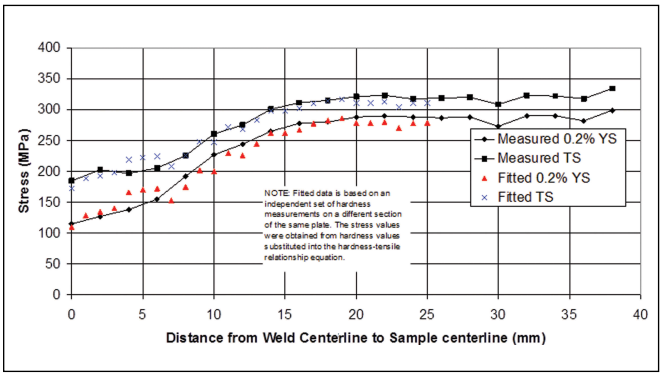

Fig. 11 — Plot of actual and predicted tensile results based on the hardness model. The hardness data for the fitted results were obtained from an independent hardness traverse of a different section of the sample, GMA weld (Plate 2A).

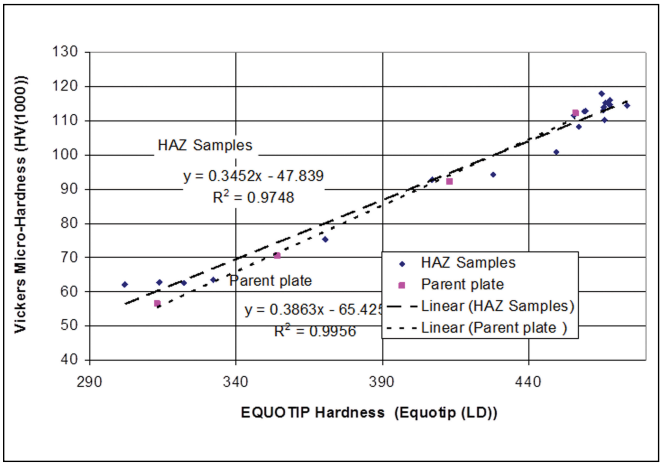

Fig. 12 — Vickers microhardness results vs. EQUOTIP results, GMA weld (Plate 2A).

Gas tungsten arc welding was conducted using a Hitachi inverter GTAW machine 300GP, model 300A AD-GPVE used in AC square wave mode. The shielding gas employed was welding grade argon at a flow rate of 5 L/min. The single-V GTAW plate was back-machined to a depth of 4 mm and three weld passes were then used to fill the weld preparation groove. In effect, this weld emerged as an unbalanced double-V weld.

Prior to welding, a distance scale was marked on the surface of the plates to measure welding travel speed in order to estimate the heat input to the work. Waveforms of the GMAW voltage were recorded at regular intervals during the welding procedure, in order to store the waveform and obtain the RMS value of the welding voltage. Welding currents and voltages were recorded manually during the procedures as summarized in Table 6. Measurements of the wire feed speed, travel speed, and other variables were recorded on the welding procedure sheet.

Radiography of Test Plate

Test plates were radiographed to choose defect-free tensile samples. Minor porosity was observed and was located principally in the weld reinforcement.

Metallographic Examination of Welds

The test plate was sectioned to provide a range of other samples including some for metallographic examination of the welds. Transverse through-section macrosections were prepared and the samples etched in Keller's reagent (2.0 mL of HNO_3, 1.5 mL of HCl, 1.0 mL of HF, and 95 mL of H_2O). This etchant revealed the

Table 6 — Summary of Welding Conditions

Plate ID	Weld Prep	Process	Filler Wire	No. of Passes	Arc RMS Voltage, V (volts)	Current I (A)	Travel Speed, S (mm/s)	Wire Feed Rate (mm/s)	Power Drawn P = I × V (kW)	Linear Energy Q = P/S(kJ/mm) (see note)
2A	Single Vee	GMAW Pulsed	4043, 1.6-mm-diam. wire	5 + 1 pass on back	3.22* nominal 20 V	185	8.1–9.7 avg. 8.9	38.7	0.596 (3.22V) 3.700 (20 V)	0.07 (3.22 V) 0.42 (20 V)
2B	Single Vee	GTAW AC	4043, 2.5-mm-diam. rod	4 + 3 passes on back	22**	230–295 avg. 263	1.45–1.95 avg. 1.7	N/A	5.786	3.4
2C	Double Vee	GMAW Pulsed	4043, 1.6-mm-diam. wire	3 per side	3.22* nominal 20 V	185	10–18.3 avg. 14.2	38.7	0.596 (3.22V) 3.7 (20 V)	0.07 (3.22 V) 0.26 (20 V)

* Voltage measured between electrode and work.
** Nominal operating voltage only.
Note – Both the measured and nominal voltages have been used to calculate the linear energy (Q). The value of 3.22 V appears to be very low compared with the nominal operating voltage.

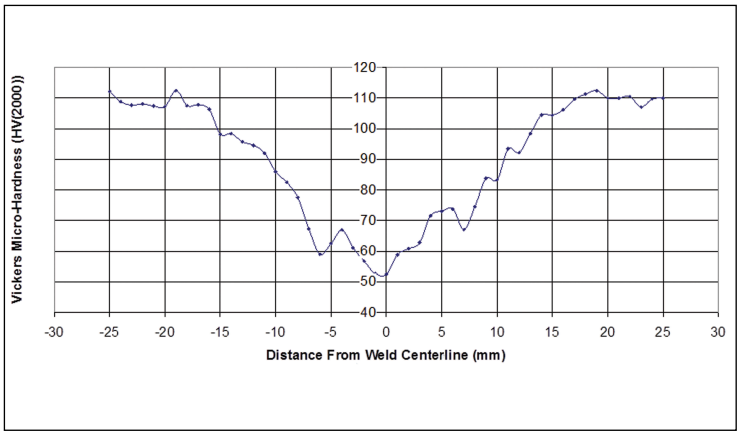

Fig. 13 — Hardness profile of midthickness single-V GMA weld (Plate 2A).

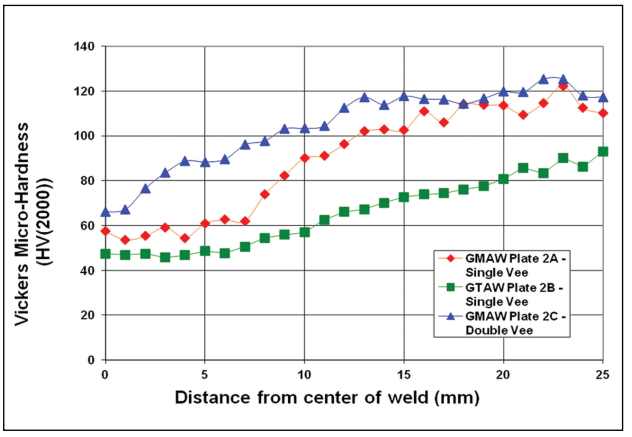

Fig. 14 — Hardness profile of single- and double-V GMA welds plus single-V GTA weld.

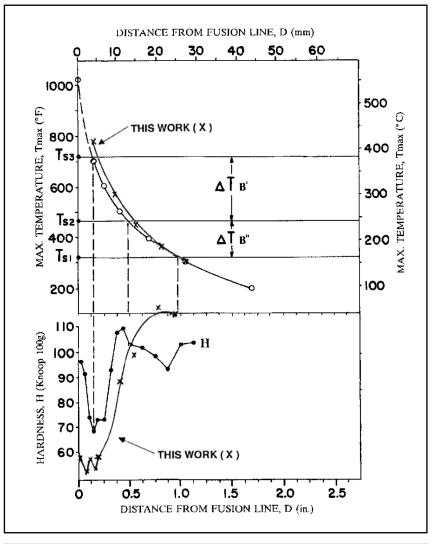

Fig. 15 — This work compared with the work of Ref. 25. (Reproduced from Welding Journal, September 1995, p. 313-s, by V. Malin.)

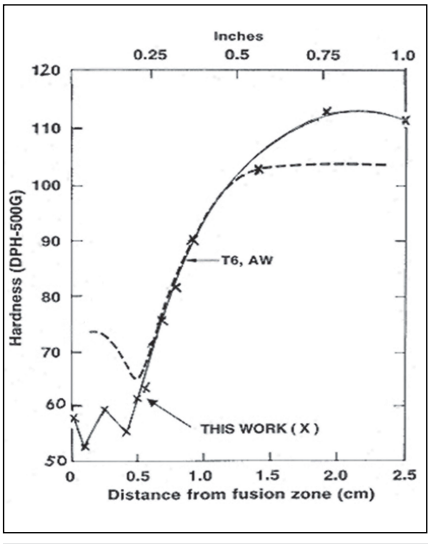

Fig. 16 — Comparison of as-welded results from The Aluminum Association (Ref. 8) with this work. (Reproduced courtesy of The Aluminum Association, Inc.)

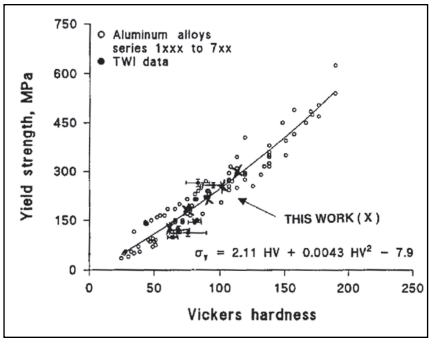

Fig. 17 — Comparison of results from this work with TWI reference (Ref. 29). (Reproduced courtesy of The Welding Institute Ltd.)

macrostructure of the weld metal and HAZ — Fig. 2.

Estimation of Weld Metal Dilution Factor

The weld filler metal (4043) will be diluted by the 6061 base material and this dilution affects the mechanical properties of the weld. This dilution factor has been estimated from the macrosections of the weld and the original weld preparation profile. The average dilution factor is 18.6% of the base plate in the weld metal. The dilution is not constant over the whole weld section; the root runs will have a higher dilution factor and the interpass runs will have a lower dilution factor due to the fact that they will be diluted by weld material that has already been diluted by the base plate; the weld reinforcement will have lowest dilution.

The dilution factor that best applies to the tensile sample test section removed from the weld metal is 13.9%.

Measurement of Temperature Profile during Welding

The temperature profile experienced by the welded test plates was measured by instrumenting the test plates with eight 0.5-mm-diameter type K thermocouples. The thermocouples were embedded to a depth of 6.35 mm (midthickness); as the two half test plates were of the same dimensions and the welding procedure was symmetrical, only one side of the assembly was instrumented. Temperature was continuously recorded during welding by a computer-based monitoring and logging system (Ref. 10).

Preparation of Tensile Samples

Two tensile testing programs were conducted:

- Tensile testing of overaged plate in both the transverse and longitudinal directions. These results were used to check the hardness–tensile relationship established by the HAZ tensile samples.
- Testing of through-thickness tensile samples that were cut (using EDM) parallel to the direction of welding. These samples were prepared in order to test thin zones of HAZ mate-

Table 7 — Summary of HAZ Tensile and Hardness Results

Sample No.	Test No.	Distance from Weld C/line	0.2%YS (MPa)	TS (MPa)	Elongation (%)	Hardness LD Side 1 Site A	Side 1 Site B	Side 2 Site C	Side 2 Site D	Average All Readings LD	Hardness Side 1 Site A	HV (1000) Side 1 Site B	Side 2 Site C	Side 2 Site D	Average All Readings HV(1000)
1	T9117	0	115	184.7	5.5	310	299	310	289	302	62.4	60.3	62.6	63.1	62.1
2	T9118	2	127	202.6	8.6	320	310	314	311	313.75	64.5	59.1	68.4	59.4	62.85
3	T9119	4	138	196.8	15.5	322	320	330	317	322.25	61.9	61.1	68.1	59.2	62.575
4	T9120	6	155	205.4	16.2	335	331	333	330	332.25	65.2	64.8	64.5	59.4	63.475
5	T9121	8	192	225.6	12.9	358	367	381	376	370.5	64.6	67.4	83.7	85.8	75.375
6	T9122	10	227	260.8	14.1	416	398	398	416	407	86.3	85.6	98.5	100.9	92.825
7	T9123	12	244	275.1	15	420	429	432	431	428	91.6	90.4	97.6	97.5	94.275
8	T9124	14	265	300.7	15.3	450	444	458	446	449.5	96.3	95.9	107.8	103.3	100.825
9	T9125	16	278	311.3	14.4	463	457	455	454	457.25	108.1	103.4	112.2	109.4	108.275
10	T9126	18	280	315	14.5	463	457	454	448	455.5	108.1	109.1	117.5	111.9	111.65
11	T9127	20	288	321.4	16	465	460	471	469	466.25	116.9	110.7	120.1	113.2	115.225
12	T9128	22	290	323.2	14.7	462	466	473	470	467.75	114.2	114.6	116	119.3	116.025
13	T9129	24	288	317.4	14.6	465	468	468	459	465	120.3	112.9	120	118.9	118.025
14	T9130	26	287	319	14.8	463	466	468	467	466	112.2	108.4	112.5	108.3	110.35
15	T9131	28	288	320	12.7	467	478	475	475	473.75	117.9	113.9	112	114.2	114.5
16	T9132	30	273	308.7	14.7	464	461	459	454	459.5	117.3	112.5	111.2	110.5	112.875
17	T9133	32	290	322.8	12.6	459	466	466	472	465.75	109.1	113.8	112	121.2	114.025
18	T9134	34	290	322.2	12.6	470	464	452	450	459	108.3	112.2	116.1	114.6	112.8
19	T9135	36	282	317.9	12.1	470	471	467	463	467.75	115.3	116.3	114.3	113	114.725
20	T9136	38	299	334.3	14.4	467	465	468	462	465.5	114.6	112.2	115.8	109.5	113.025

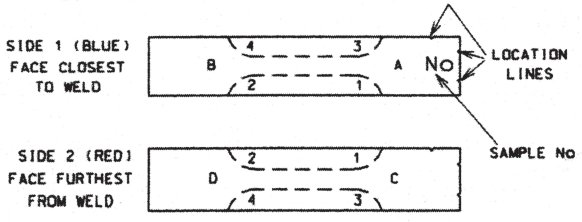

HARDNESS MEASUREMENT SITES A–D AND 1–4 (BOTH SIDES)

rial and establish the hardness–tensile property relationships.

Tensile Samples from Overaged Base Plate

Tensile samples were prepared from the four overaged 6061 plates. These samples were prepared in accordance with Australian Standard AS 1391-1991 (Ref. 27). The sample design is shown in Fig. 3 and the location from which the samples were cut is shown in Fig. 4. The samples were tested on an INSTRON 8501 servo-hydraulic testing machine at a strain rate of 8×10^{-5}/s and in accordance with AS 1391-1991.

Electric Discharge Machined Samples Extracted from the HAZ

Samples were extracted from the single-V GMA weld plate (Plate 2A). Through-thickness tensile sample blanks were electric discharge machined (EDM) from the plate, starting from the center of the weld metal and progressing away from the weld at 2-mm intervals, to a distance of 40 mm from the weld. A series of 20 samples at 2-mm intervals from the centerline of the weld was prepared, with particular care taken to ensure there were no sequencing or orientation errors, nor any bending or deformation. Figure 5 shows the extraction procedure and cutting layout for the welded test plate. The test section is small and the thermal difference across the test section is also believed to be small.

The above process produced sample blanks that were approximately 1.7 mm thick, 65 mm long, and 12.7 mm wide. The width of the EDM wire cut was approximately 0.3 mm. Electric discharge machining is performed at room temperature; however, there is a damaged layer resulting from the electric discharge. These damaged layers were removed by hand grinding both sides of each specimen blank on wet silicon carbide papers. Figure 6 shows a drawing of the HAZ tensile samples.

Table 8 — Summary of Fitted Equations for Tensile – EQUOTIP Hardness Relationship (Results Should Be Rounded to Nearest MPa)

Data Group	Regression Fitted Equation to Data	Coefficient of Determination (R^2)
HAZ 0.2% YS	Y = 1.035x – 194.79	0.9927
HAZ TS	Y = 0.8424x – 73.529	0.98
Parent 0.2% YS Transverse	Y = 1.2687x – 282.05	0.9978
Parent TS Transverse	Y = 0.9621x – 115.46	0.9993
Parent 0.2% YS Longitudinal	Y = 1.4111x – 335.48	0.999
Parent TS Longitudinal	Y = 0.9614x – 118.8	0.9961

Hardness Testing of All Samples

Vickers microhardness and EQUOTIP hardness testing were performed on all samples and heat-treated test plates. Overaged base plate material was hardness tested in two locations on each sample using both a Leco model M-400-H2 Vickers microhardness testing machine and an

Table 9 — Summary of Fitted Equations for Tensile – Vickers* Hardness Relationship (Results Should Be Rounded to Nearest MPa)

Data Group	Regression Fitted Equation to Data	Coefficient of Determination (R^2)
HAZ 0.2% YS	Y = 2.9263x – 44.289	0.9703
HAZ TS	Y = 2.4079x + 46.39	0.979
Parent 0.2% YS Transverse	Y = 3.2637x – 65.518	0.99
Parent TS Transverse	Y = 2.4828x + 48.1266	0.9974
Parent 0.2% YS Longitudinal	Y = 3.6337x – 94.949	0.993
Parent TS Longitudinal	Y = 2.4848x + 44.32	0.9976

*Vickers microhardness HV (average of 1000 g and 2000 g).

EQUOTIP hardness tester. Loads of 1 and 2 kg were used for the Vickers measurements and the average of all four readings taken; individual readings varied by no more than ±2 Vickers microhardness units for both loads and all readings. Hardness readings were also taken using the full-size Vickers diamond indentation method and these readings were also within ±2 Vickers units of the micro-Vickers measurements. An average of 12 readings, 6 on each side, was taken using the EQUOTIP hardness tester with the 'D' indenter.

Hardness measurements were also made using the Leco microhardness tester and the EQUOTIP hardness tester on all 20 through-section HAZ tensile samples. Average readings from two sites on each side of each sample were taken. The hardness sites were at approximately the midthickness of the plate in order to obtain hardness readings that were as close to either end of the tensile test section as possible, so that the indentations did not influence the tensile properties.

Tensile Testing of Through-Thickness HAZ Samples

These samples were tested on an INSTRON 8501 servo-hydraulic testing machine fitted with a 5-kN calibrated load cell and the data logged using purpose-written software. A 10-mm gauge length extensometer with a 1-mm range was attached to the sample, allowing sample strains up to 10% to be measured. The extensometer was calibrated prior to use and was found to have a linear error of 2.25%, this being corrected in software to better than 0.5% accuracy. Data logging included the time, extensometer reading, load, and cross-head position. The tensile testing conditions were the same as those used for testing the overaged 6061 tensile samples. A 0.2% offset strain was used to determine the yield strength.

The tests were conducted in accordance with AS 1391-1991. The 0.2% yield stress (YS), tensile strength (TS), and elongation were measured on each sample. The samples were tested in strain control up to approximately 2% strain at an extension rate of 0.001 mm/s, which gave a strain rate of 1×10^{-4}/s (AS 1391 L1 strain rate range). After 2% strain the machine was switched to position control and run at 0.05 mm/s until sample fracture.

Results

Overaged Base Plate Tensile and Hardness Test Results

Tensile and hardness results for samples extracted from the overaged base plates are shown in Figs. 7 and 8. Results for longitudinal 0.2% yield and tensile strengths as a function of measured EQUOTIP and Vickers hardnesses are shown in Fig. 7. Results for transverse 0.2% yield and tensile strengths as a function of measured EQUOTIP and Vickers hardnesses are shown in Fig. 8. Longitudinal and transverse elongation, as well as reduction of area, were obtained as a function of measured EQUOTIP and Vickers hardnesses. These results are considered to be outside the scope of this paper, but are contained in Ref. 10 (this dissertation may be borrowed on interlibrary loan from the ANSTO or University of Wollongong Libraries).

Description of Weld Macrosections

Macroetching successfully revealed the weld runs and HAZ of the weld section. Some porosity was visible in the weld, this being consistent with the radiographs taken of the test plate. As mentioned previously, the porosity was mainly confined to the reinforcement. Some misalignment of the run on the reverse side exists and this is plainly visible in the macrograph. Misalignment of the two plates, due to distortion, occurred and was in the order of 1 mm; this was not considered important for the remainder of the experiment. A high level of porosity was evident in the reinforcement of the backing pass. This region of the weld was subsequently machined away.

Tensile and Hardness Results for HAZ Samples Extracted from GMA Weld (Plate 2A)

A summary of the tensile results and hardness measurements is shown in Table 7. The diagram at the bottom of the table indicates the location of the hardness tests; such measurements were taken on both sides of each tensile blank. Both EQUOTIP and Vickers microhardness measurements were taken at sites A, B, C, and D (with sufficient spacing to ensure no interaction).

Reference 10 contains the tensile curves for all test samples; the 0.2% yield stress graph and complete tensile graph are shown as separate graphs. The tensile curves were produced with the extensometer attached to a strain of 10%, which is its nominal limit. These curves have been retained in this work because they may be useful for future finite element modeling of the HAZ behavior; the data can also be made available in electronic format. Some high-elongation curves will be truncated due to the extensometer reaching its stops before failure occurred. The cross-head position was also logged; however, these data were not plotted. All results in this section are related to the single-V GMA weld test Plate 2A. All the results shown in Figs. 9–14 are taken from Ref. 10.

Discussion

Hardness was found to accurately predict the yield strength (0.2% offset YS) and tensile strength (TS) in welded 6061-T651 test plates — Fig. 11. Separate hardness profiles were conducted on another section of the GMA weld (Plate 2A) and found to be in good agreement with measured values. The test results from Plate 1 (Table 2) which had been overaged to four hardness levels, show that the standard size tensile and hardness results compared well with those of the HAZ samples. This indicates that the use of subsize tensile samples from the HAZ did not affect the accuracy of the results. The agreement between Plate 1 results and the HAZ sample results was found to be very good — Fig. 12. Only the transverse results from the base plate have been used for comparison purposes as this was the same orientation as the miniature HAZ tensile samples. The longitudinal tensile results from the base plate gave slightly higher results than the transverse results. If hardness results are to be used to estimate tensile properties in both the longitudinal and transverse directions for the purposes of finite element modeling, then it is worth making the corrections to obtain longitudinal results. Hardness test methods used in this work do not discriminate between longitudinal and transverse hardness. For this reason, it is important to establish transverse–longitudinal property ratios if an additional degree of accuracy is required.

Comparisons between fitted and actual results for the tensile–hardness relationship showed a linear correlation. The correlation was very good (coefficient of determination >0.99) for the overaged base plate samples, and slightly lower for the HAZ samples (~0.98). The increased variation in the HAZ samples is probably a real effect, and may reflect variations in the weld metal and HAZ; observations of the etched macrosections indicate that subsequent weld passes had modified the structure of underlying weld passes, and variations in the dilution factor may also affect the results.

It would appear that the rate of heating does not influence the hardness–tensile relationship. The HAZ results were obtained with heating rates typical of the welding process and heating took place in the order of seconds. The hardness–tensile relationship obtained from these results gave very similar results to those obtained from the overaged base plate material that was heated to lower temperatures for longer times. It would appear that overaging might be described by a single time–temperature parameter and an opportunity may exist to study this phenomenon; however, this is beyond the scope of the present work.

Tables 8 and 9 provide a summary of the linear regression fitted lines to the experimental data for the EQUOTIP and Vickers hardness–tensile properties relationship, for both the HAZ and base plate samples. Hardness values (x) can be substituted into these equations to obtain YS or TS. The R-squared value is also shown as an indication of the percentage of the response variable variation that is explained by the linear model, and as can be seen this is excellent, a value of 1 (100%) indicating a perfect fit.

Comments on the Shape of the Curves

It will be observed from this work and that of others that as the distance from the weld interface of the weld increases, the hardness drops, reaches a minimum, and then increases again progressively to the original base plate hardness. Figure 13 shows that the hardness increases at a distance of about 5 mm from the centerline of the fusion zone, which corresponds to the location of the fusion zone edge. The explanation for this characteristic shape is given by Malin (Ref. 25). At the weld interface, the precipitates of β″ and β′ are dissolved at the high temperature and enrich the solid solution with Si and Mg, which results in solid-solution hardening of the matrix. As the distance increases, a minimum hardness is reached and then the hardness increases again. In this area, the HAZ is experiencing progressively lower temperatures as the distance from the weld increases. The degree of hardness reduction is proportional to the distance from the weld; that in turn is proportional to temperature, and this is related to the coarsening of the β″ precipitates. β″ precipitates increase in size with increasing temperature, and this weakens the structure and reduces hardness. Figure 10 shows the maximum elongation is also obtained at about 5 mm from the weld centerline, and this corresponds to the weld interface where the structure is closest to the fully solution-treated state.

In Fig. 9, which shows HAZ hardness vs. tensile strength, the results for the HAZ are a good fit for a linear relationship between strength and hardness; however, the results for the samples extracted from the weld metal do not fit the straight line plot for the HAZ. The hardness–strength relationship shows hardness reaches an approximately minimum value and remains constant. This effect is thought to be the result of a complex interaction of thermal effects and dilution factor in the weld zone.

Figure 10, a plot of strength and elongation as a function of distance from the weld centerline, shows that the strength returns to base plate values at a distance of approximately 20 mm from the weld centerline for Plate 2A. The elongation has a minimum of approximately 5% near the center of the weld and reaches a maximum of approximately 16% near the weld interface; the material properties in this region are more characteristic of the 4043 filler metal modified by the dilution from the base plate.

Figure 14, which contains plots of hardness vs. distance from the weld centerline, shows the effect of heat input resulting from different weld preparations and welding methods. The single-V GTA weld has the highest heat input, resulting in lower hardnesses for a greater distance from the weld centerline compared to the single- and double-V GMA welds; the double-V GMA weld with the lowest total heat input shows the highest hardnesses and least overall reduction in strength in the HAZ.

Comparison with Other Results

No direct comparison with this work was found for 6061-T6 or 6061-T651 aluminum. This work involved a systematic study of thin sections of HAZ material as a function of distance

from the weld and included the measurement of hardness. Malin (Ref. 25), however, has carried out a thorough and systematic study of the Knoop hardness and microstructural properties of welds in 6061 aluminum as a function of distance from the weld. The study also included cross-weld tensile tests, and compared the fracture location and tensile properties with the hardness at that location in the weld. From these results, conclusions were drawn about the hardness–tensile relationship. This approach, naturally, gives only one tensile result per weld. Malin's welds were also 6061-T6 using 4043 filler metal and the GMAW method; however, the welds were performed on extruded sections that were thinner than those used in the present work.

As a comparison with the present work, Fig. 15 has been reproduced from Malin's work with the present results, converted to Knoop hardness using the conversion tables in ASTM E 140 (Ref. 28), superimposed on the diagram. Malin used three different heat input values and the results shown are for the heat input closest to this work, i.e., corresponding to a current of approximately 185 amps.

Also shown on Malin's diagram in Fig. 15 is the temperature profile as a function of distance from the weld interface. The present temperature results, taken from Ref. 10, for the root run of the GMA weld (Plate 2A) have been superimposed on this diagram for comparison. The root weld run also produced the highest temperature on that plate.

The hardness results are in reasonable agreement with Malin's work, with hardnesses extending above and below his results. This may be explained by the difference in section thickness used to produce the different welds. The magnitude of the hardness peak close to the weld interface was not as high as that observed by Malin. This was possibly due to the influence of thermal modification of the structure resulting from subsequent weld passes; Malin's work involved a single weld pass. The temperature profile results are very close to those of Malin's work.

Other work was referenced in *Welding Aluminum: Theory and Practice* (Ref. 8) and gave a relationship between distance from the weld and the hardness. This has been reproduced in Fig. 16 and the present results are superimposed on the graph. At distances of approximately 5–12 mm from the weld, the present work gives a very close approximation for both distance and hardness values. As with the comparison with Malin's work, lower hardnesses were observed close to the weld and higher hardness was measured close to the weld interface. This weld was produced using the GTAW process with no details of filler metal given. The higher hardness close to the weld interface was not observed to the same degree; this was possibly due to thermal modification of the structure by subsequent weld passes.

The Welding Institute (TWI) has produced a graph of hardness vs. yield strength for all aluminum alloys from 1XXX to 7XXX (Ref. 29). The present yield strength results for 6061-T651 aluminum were superimposed on the TWI graph (Fig. 17), and were found to be very close to the fitted line for all alloys. This is an interesting result because the HAZ samples from the present work were a mixture of Al-Si alloy (4043 filler) and 6061 alloy, and the hardness–tensile relationship appeared to hold reasonably well for all samples.

Comparison with the work of others (Refs. 8, 25, 29) indicates that the results obtained in this work correlate well with published data. An extensive literature review did not reveal a directly comparable study performed in a similar manner to this work. Most of the tensile results uncovered were cross-weld results, and from these results, conclusions were drawn about the hardness–tensile property relationship in 6061 aluminum. The present work has extracted miniature samples from the HAZ and made direct measurements of tensile and hardness properties on small zones of the HAZ and weld metal.

Conclusions

Hardness was found to be a reliable method of estimating the yield and tensile strength of the heat-affected zone (HAZ). A relationship between hardness and tensile properties was established for both Vickers microhardness and EQUOTIP portable hardness testing. These relationships have been expressed mathematically as follows:

Vickers Microhardness

0.2% Yield stress = 2.9263 HV – 44.289

Tensile strength = 2.4079 HV + 46.39

EQUOTIP Portable Hardness Tester (D indenter)

0.2% Yield stress = 1.035 LD – 194.79

Tensile strength = 0.8424 LD – 73.529

Notes: Stress values are in MPa (and should be rounded to the nearest MPa).

HV Vickers microhardness diamond indenter hardness values.

LD is Leeb units produced with the EQUOTIP D indenter.

Although the relationships were established with Vickers microhardness indenters, comparison between Vickers microhardness and full-size hardness results indicate that the above relationships should hold for full-size Vickers hardness tests.

The tensile data obtained from the sections of HAZ could be useful for finite element modeling of weld-zone behavior, and all curves have been retained.

The hardness–tensile model established for 6061 aluminum welded with 4043 will be useful in establishing the extent of the HAZ, and assigning tensile properties to regions within this zone based on hardness measurements. From a practical standpoint, hardness measurements are quicker and more straightforward than numerical calculation of the HAZ properties.

Acknowledgments

The authors wish to thank the Australian Nuclear Science and Technology Organisation (ANSTO) for the provision of project funding, laboratory facilities, and development workshop support, as well as the Cooperative Research Centre for Welded Structures (CRC-WS) at the University of Wollongong, Australia,

for offering the Master of Engineering Practice Degree in Materials Welding and Joining undertaken by P. A. Stathers. Appreciation is also expressed to Associate Professor S. R. Yeomans from the Australian Defence Force Academy (ADFA) for sharing his ideas for this work.

References

1. Porter, D. A., and Easterling, K. E. 1992. *Phase Transformations in Metals and Alloys,* 2nd ed. London, UK: Chapman and Hall.

2. Dumolt, S. D., Laughlin, D. E., and Williams, J. C. 1984. Formation of a modified β′ phase in aluminum alloy 6061. *Scripta Metallurgica et Materialia* 18(12): 1347–1350.

3. Enjo, T., and Kuroda, T. 1982. Microstructure in weld heat affected zone of Al-Mg-Si alloy. *Transactions of JWRI (Japanese Welding Research Institute)* 11 (61): 61–66.

4. Dickerson, P. B., and Irving, B. 1992. Welding aluminum: it's not as difficult as it sounds. *Welding Journal* 71(4): 44–50.

5. Welding Technology Institute of Australia. 1997. Successful Welding of Aluminium. *WTIA Technical Note TN 2-97*, 3rd ed. Lidcombe, NSW.

6. Yeomans, S. R. 1997. HAZ softening in welded aluminium alloys — its causes and significance in design. *Australasian Welding Journal* 42(3): 16–18.

7. Yeomans, S. R. 1996. Welding in Structural Engineering: Steels and Aluminium Alloys. Short Course. Canberra, ACT, Australia: University of New South Wales.

8. Saunders, H. L. 1991. *Welding Aluminum: Theory and Practice*, 2nd ed., June. Arlington, Va.: The Aluminum Association, Inc.

9. Cottrell, A. 1995. *An Introduction to Metallurgy*, 2nd ed., p. 438. London, UK: The Institute of Materials.

10. Stathers, P. A. 2000. Welding of 6061-T651 aluminium and the relationship of tensile properties to hardness in the heat affect zone. Master of Engineering Studies dissertation. Wollongong, NSW, Australia: University of Wollongong.

11. Myhr, O. R., and Grong, Ø. 1991. Process modelling applied to 6082-T6 aluminium weldments—I. Reaction kinetics. *Acta Metallurgica et Materialia* 39(11): 2693–2702.

12. Myhr, O. R., and Grong, Ø. 1991. Process modelling applied to 6082-T6 aluminium weldments—II. Applications of model. *Acta Metallurgica et Materialia* 39 (11): 2703–2708.

13. Shercliff, H. R., Grong, Ø., Myhr, O. R., and Ashby, M. F. 1992. Process modelling applied to age hardening aluminium alloys. *ICAA3: Proc. 3rd Int. Conf. on Aluminium Alloys – Their Physical and Mechanical Properties*. Norwegian Institute of Technology, University of Trondheim, Trondheim, Norway, 22-26 June, Eds. L. Arnberg, O. Lohne, E. Nes, and N. Ryum, 2nd ed., vol. III, pp. 357–369.

14. Andersen, I., and Grong, Ø. 1995. Analytical modelling of grain growth in metals and alloys in the presence of growing and dissolving precipitates—I. Normal grain growth. *Acta Metallurgica et Materialia* 43(7): 2673–2688.

15. Andersen, I., Grong, Ø., and Ryum, N. 1995. Analytical modelling of grain growth in metals and alloys in the presence of growing and dissolving precipitates—II. Abnormal grain growth. *Acta Metallurgica et Materialia* 43(7): 2689–2700.

16. Grong, Ø. 1997. Metallurgical modelling of welding of aluminium alloys. *Mathematical Modelling of Weld Phenomena 3*. Eds. H. Cerjak, and H. K. D. H. Bhadeshia, pp. 313–356. London, UK: The Institute of Materials.

17. Grong, Ø. 1997. *Metallurgical Modelling of Welding*, 2nd ed. London, UK: The Institute of Materials.

18. Bjørneklett, B. I., Grong, Ø., Myhr, O. R., and Kluken, A. O. 1999. A process model for the heat-affected zone microstructure evolution in Al-Zn-Mg weldments. *Metallurgical and Materials Transactions A* 30A (10): 2667–2677.

19. Myhr, O. R., Grong, Ø., and Andersen, S. J. 2001. Modelling of the age hardening behaviour of Al-Mg-Si alloys. *Acta Materialia* 49(1): 65–75.

20. Grong, Ø. 2001. New trends in mathematical modelling of aluminium alloys. *Mathematical Modelling of Weld Phenomena 5*. Eds. H. Cerjak, and H. K. D. H. Bhadeshia, Session 3, pp. 401-420. London, UK: The Institute of Materials.

21. Myhr, O. R., Grong, Ø., Klokkehaug, S., and Fjaer, H. G. 2002. Modelling of the microstructure and strength evolution during ageing and welding of Al–Mg–Si alloys. *Mathematical Modelling of Weld Phenomena 6*. Eds. H. Cerjak, and H. K. D. H. Bhadeshia, Session 3, pp. 337-363. London, UK: Maney Publishing (for The Institute of Materials, Minerals and Mining).

22. Myhr, O. R., Grong, Ø., Fjaer, H. G., and Marioara, C. D. 2004. Modelling of the microstructure and strength evolution in Al-Mg-Si alloys during multistage thermal processing. *Acta Materialia* 52(17): 4997–5008.

23. Myhr, O. R., and Grong, Ø. 2008. Utilizing a predictive tool for designing welded aluminum components. *Welding Journal* 87(5): 36–39.

24. Myhr, O. R., and Grong, Ø. 2009. Novel modelling approach to optimisation of welding conditions and heat treatment schedules for age hardening Al alloys. *Science and Technology of Welding and Joining* 14(4): 321–332.

25. Malin, V. 1995. Study of metallurgical phenomena in the HAZ of 6061-T6 aluminum welded joints. *Welding Journal* 74 (9): 305-s to 318-s.

26. Standards Australia. 1979. *SAA Aluminium Structures Code*, AS 1664-1979. North Sydney, NSW.

27. Standards Australia. 1991. *Methods for Tensile Testing of Metals*, AS 1391-1991. North Sydney, NSW.

28. American Society for Testing and Materials. 1984. *Standard Hardness Conversions for Metals*, ASTM Designation E 140-84. Philadelphia, Pa.

29. Wiesner, C. S., and Gittos, M. F. 1994. Relationship Between Tensile Strength and Hardness for all Aluminium Alloys. Unpublished TWI Report, TWI 620413/1/94, p. 14. Granta Park, Great Abington, Cambridge, CB1 6AL, UK, The Welding Institute Ltd.

AWS Expands International Services

With international membership on the rise, the American Welding Society (AWS) launched a series of country-specific Web sites known as microsites for members to access information in their native languages.

Multilingual microsites are now live for Mexico at *www.aws.org/mexico*, China at *www.aws.org/china*, and Canada (English/French) at *www.aws.org/canada*. They feature information on services offered by AWS in each country, membership benefits, exposition information, online education, and access to AWS publications and technical standards.

Other countries will be added later.